Wave-induced Doppler Shift of Ka-band Radar Signal Backscattered from the Sea Surface

Yu. Yu. Yurovsky[1], **S. A. Grodsky**[2], **V. N. Kudryavtsev**[1,3], **and B. Chapron**[4]

[1]FSBSI Marine Hydrophysical Institute RAS, Russia
[2]Department of Atmospheric and Oceanic Science, University of Maryland, USA
[3]Russian State Hydrometeorological University, Russia
[4]Institut Français de Recherche pour l'Exploitation de la Mer, France

Abstract— The Wave-Induced Doppler velocity (WIDV) arising from correlated modulations of sea surface velocity and its normalized radar cross-section (NRCS) is evaluated from Ka-band radar measurements taken from the Black Sea research platform. The WIDV measurements are compared to the WIDV simulations using an empirical Ka-band Modulation Transfer Function (MTF) and wind wave spectrum parameterization zeroed at frequencies below the observed peak frequency to account for fetch-limited waves typical of the Black Sea. Given a good agreement between measured and simulated WIDV, we extrapolate the WIDV onto the open ocean conditions by using the fully developed wave spectrum. Simulated open ocean WIDV depends on incidence angle, azimuth, radar polarization, and wind speed. The WIDV magnitude has a peak at small incidence angles ($\theta = 20°$), with downwind magnitude larger than upwind magnitude. At larger θ, the WIDV decreases. The wind speed dependence of WIDV is explained by two competing factors, MTF decrease with the wind and peak wave orbital velocity amplification with the wind. The typical magnitude of WIDV is 3 to 8 times larger than either Bragg wave phase velocity or wind drift velocity for winds between 5 m/s and 15 m/s. Thus, the WIDV is important for the sea surface currents retrieval from satellite Doppler radar measurements.

1. INTRODUCTION

Doppler shifts of microwave radar backscattering from the sea surface allow for high-resolution measurements of ocean currents from aircrafts or satellites [1]. Future Doppler scatterometer missions [2, 3] are planned to operate in the Ka-band in order to achieve a better measurement accuracy. Although Doppler signatures of ocean backscatter have been studied both theoretically [4–6] and experimentally [7–9], the mean Doppler shift in the Ka-band is not well documented yet.

Doppler frequency shift, or corresponding Doppler Velocity (DV), results from a combination of i) surface currents, ii) inherent scatterer movements, and iii) orbital wave motions. The first term is the target term that needs to be determined from observations. The second term depends on the particular backscattering mechanism and can be estimated theoretically, e.g., Bragg wave phase speed for the resonant backscattering, mirror point velocity for specular reflections [10]. The third term is a Wave-Induced Doppler velocity (WIDV) that occurs due to correlated modulations of local sea surface velocity and Normalized Radar Cross-Section (NRCS) [11]. Proper description of the WIDV is principal for the extracting of the surface currents from measured DV. Assuming that local velocities are determined by the wave orbital velocity only, the WIDV estimation requires the knowledge of NRCS modulation characteristics.

Radar Modulation Transfer Function (MTF), which relates surface wave parameters with radar signal modulations, has been studied intensively in order to understand the mean NRCS and the imaging mechanism of waves resolved by radars [12–14]. In the present study, the WIDV is estimated using an empirical Ka-band MTF [15]. We compare these estimates with multi-year Ka-band radar observations from a research platform in the Black Sea. For open ocean conditions, Ka-band WIDV is estimated using a theoretical model of the wind wave spectrum.

2. THEORY

Assuming that sea surface can be represented as an ensemble of incoherent scatterers advected by currents and waves longer than scatterer size, long waves (LW) hereinafter, and assuming that the surface current and scatterer velocity is constant within the radar footprint, the spatial mean of the line-of-sight Doppler Velocity (DV) can be written as [11],

$$v = ([\mathbf{v}_c + \mathbf{v}_s + \overline{\sigma' \mathbf{u}'}/\overline{\sigma}] \cdot \mathbf{k}_r)/|\mathbf{k}_r|, \quad (1)$$

where $\mathbf{v}_c$ is the surface current (drift) vector, $\mathbf{v}_s$ is the inherent scatterer velocity vector, $\mathbf{k}_r$ is the radar wave vector, $\mathbf{u}'$ is orbital velocity vector, $\sigma = \overline{\sigma} + \sigma'$ is the sea surface NRCS, represented as the sum of mean level and variation, round brackets $(\cdot)$ denote dot product.

For the sake of simplicity, we consider a unidirectional wave spectrum with LW co-aligned with the wind direction. In this case (1) transforms to,

$$v = v_c \sin\theta \cos\phi_c + v_s \sin\theta + |G|\overline{\sigma' u'}/\overline{\sigma}, \tag{2}$$

$$G = \cos\phi \sin\theta + i\cos\theta \tag{3}$$

where ϕ_c is the radar-to-current azimuth angle, ϕ is the radar-to-wind(wave) azimuth angle, θ is the incidence angle, G is the geometrical coefficient projecting wave orbital velocity vector onto the radar wave vector direction.

The last term in (2) is the Wave-Induced DV (WIDV). It can be obtained by subtracting the first two terms (surface current and scatterer velocity) from the total measured DV,

$$\text{WIDV} = |G|\overline{\sigma' u'}/\overline{\sigma} = v - v_c \sin\theta \cos\phi_c - v_s \sin\theta. \tag{4}$$

The surface current, $\mathbf{v}_c$, is measured either directly (by video tracking) or as a combination of 10 m depth "background" current and wind shear in the upper 10 m.

The scatterer velocity, $\mathbf{v}_s$, depends on the backscattering mechanism. At moderate incidence angles, $\theta > 30°$, the scatterers are Bragg wave patches moving at the Bragg wave phase speed,

$$c_{br} = (g/k_{br} + \gamma k_{br})^{1/2}, \tag{5}$$

where $k_{br} = 2k_r \sin\theta$ is the Bragg wave number, g is the gravity acceleration, γ is the surface tension coefficient. By replacing the inherent scatter velocity by the resonant Bragg speed component only, one disregards the velocity component associated with wave breaking scattering, which is increasingly important at larger incidence angles (see [10] for more details). Note also, that wave breaking effect is included in our empirical MTF, which is based on observations.

At small incidence angles, $\theta < 30°$, specular reflections from patches normal to the line-of-sight direction contribute as well. The size of these patches should be greater than at least a few radar wave lengths. The mean velocity of these scatterers is the mean phase velocity of carrying waves [10, 16], weighted by their spectral density and radar cross-section of mirror points. The phase speed of wind waves is higher than ≈ 23 cm/s, which is close to Bragg wave phase speed for Ka-band, 23 cm/s $< c_{br} <$ 35 cm/s, at $3° < \theta < 90°$. Thus, we use Bragg wave phase velocity as the lower limit for mean specular point velocity and suppose that $v_s = c_{br}$ for all incidence angles. Note, this assumption may somewhat underestimate v_s at small θ, and thus overestimate the WIDV (4) for small incidence angles.

On the other hand, the WIDV can be retrieved from LW spectrum, if the Modulation Transfer Function (MTF) is known. By definition, the MTF relates NRCS variations, σ', with LW slopes, ζ,

$$M = \frac{\sigma'}{\overline{\sigma}\zeta}, \tag{6}$$

Expanding variations of NRCS, σ', and orbital velocity, u', into a Fourier series of LW slope, ζ, and assuming that M is independent of LW frequency, the WIDV is expressed via the third moment of LW elevation spectrum [1, 3]

$$\text{WIDV} = g^{-1}\text{Re}\{G^* M \int \omega^3 S(\omega) \mathrm{d}\omega\}, \tag{7}$$

where ω is the LW radial frequency, and $S(\omega)$ is the LW elevation spectrum.

The WIDV is estimated using the empirical Ka-band MTF [15] and the wind wave spectrum proposed in [17] and further developed in [18, 19] by Kudryavtsev et al., the KMC spectrum hereinafter.

3. EXPERIMENT

Field measurements were conducted in 2009–2015 from the Black Sea research platform using a Ka-band real aperture continuous wave radar operating at VV and HH polarizations (calibration details

are given in [20]). The radar footprint size of a few meters allowed to resolve energy containing wind waves (peak wavelength ≈ 40 m). Empirical MTF was estimated from observed σ' and using DV as a proxy for wave elevations [15].

In-phase and quadrature components of radar backscattering at VV and HH polarizations are transformed into instantaneous NRSC, $\sigma(t)$, and DV, $v(t)$ [21]. Assuming that spatial and temporal mean values are equivalent, the mean DV (2) is computed from temporal records of σ and v,

$$v = \frac{\overline{\sigma(t)v(t)}}{\overline{\sigma(t)}}, \tag{8}$$

where the overbar stands for temporal averaging.

The wind drift shear in the upper 10 m column is estimated from synchronous measurements of 10 m current, $\mathbf{v}_{10}$, and surface current (estimated from bubble video tracking). It has been found that the current in the upper 10 m accounts for almost the entire wind drift, is directed along the wind, $\mathbf{U}$, and proportional to its speed, $\mathbf{v}_c = \mathbf{v}_{10} + 0.023\mathbf{U}$ (Fig. 1).

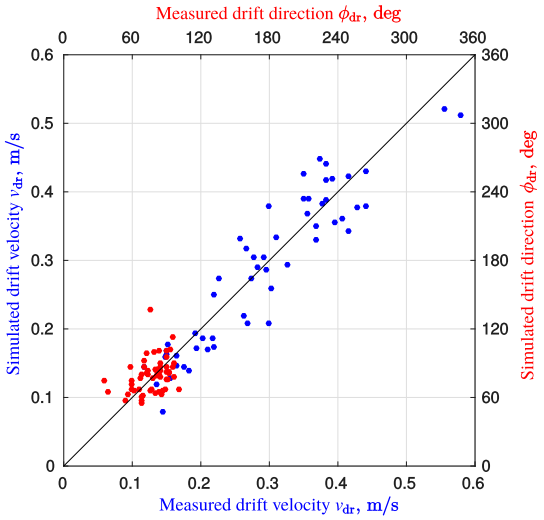

Figure 1: Wind drift measured from bubble video tracking versus wind drift simulated from a linear combination of background 10 m depth current and wind speed, $\mathbf{v}_c = \mathbf{v}_{10} + 0.023\mathbf{U}$.

4. RESULTS

4.1. Measured WIDV

The measured WIDV, estimated from (4), depends on the incidence angle (Fig. 2) and azimuth (Fig. 3). At moderate $30° < \theta < 50°$, its magnitude is of the same order as the line-of-sight Bragg wave phase velocity. It peaks at $\theta \approx 20°$ reaching about ± 0.5 m/s in the upwind and downwind directions (Fig. 2). HH WIDV is generally stronger in magnitude than that at VV polarization. At large $\theta > 60°$, HH WIDV grows rapidly up to 0.7–0.9 m/s in the upwind direction (Fig. 2b), while in the crosswind direction it vanishes at both polarizations. The azimuth dependence is more pronounced at HH polarization (Fig. 3).

4.2. Measurements vs Simulations

The measured WIDV (4) is compared to the simulated WIDV (7) using the KMC spectrum model as an input. The KMC spectrum includes the high frequency part (Fig. 4) that adequately reproduces optical measurements [19]. The low frequency part of KMC spectrum is adopted from an empirical spectrum proposed in [22]. The total spectrum is tuned to be consistent with the sea surface mean squared slope [23]. To match KMC spectra with observed fetch-limited Black Sea wave spectra, the KMC spectrum is truncated at $f < f_p$, where f_p is the measured wave peak frequency.

Although measured and simulated WIDV agree well (Fig. 5), some deviations are evident. In particular, "cyan-to-yellow" points corresponding to simulated WIDV in the crosswind direction are offset (Figs. 5(a), 5(b)). For the sake of simplicity, we assume a sharp transition of Bragg

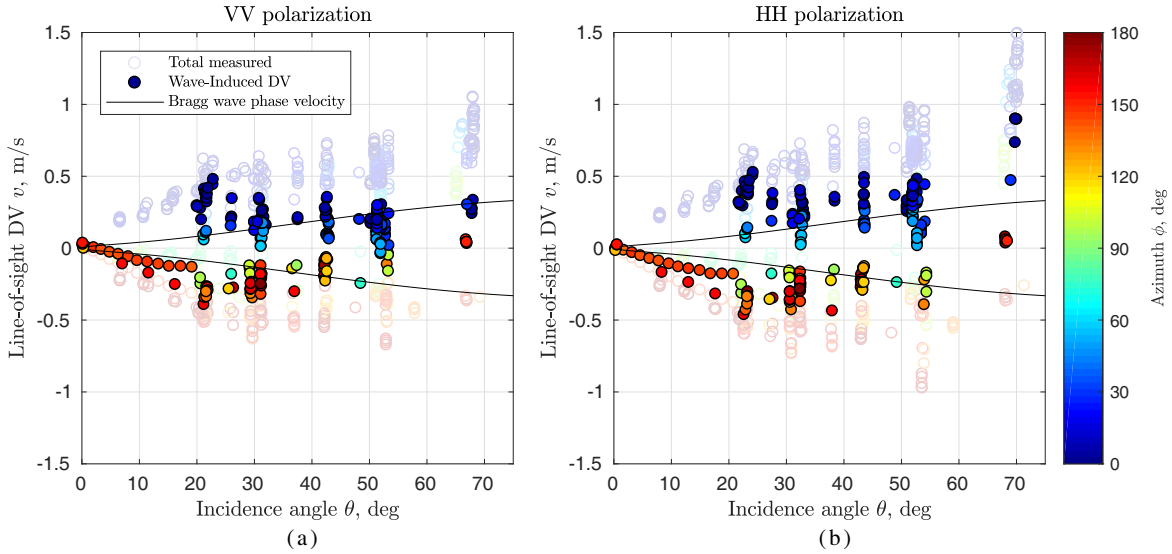

Figure 2: Measured line-of-sight Doppler velocity (DV) versus incidence angle, θ, for (a) VV and (b) HH polarization. Transparent empty circles are total measured DV, filled circles are Wave-Induced DV estimated from (4). Black solid line is the line-of-sight Bragg wave phase velocity, $c_{\rm br} \sin\theta$.

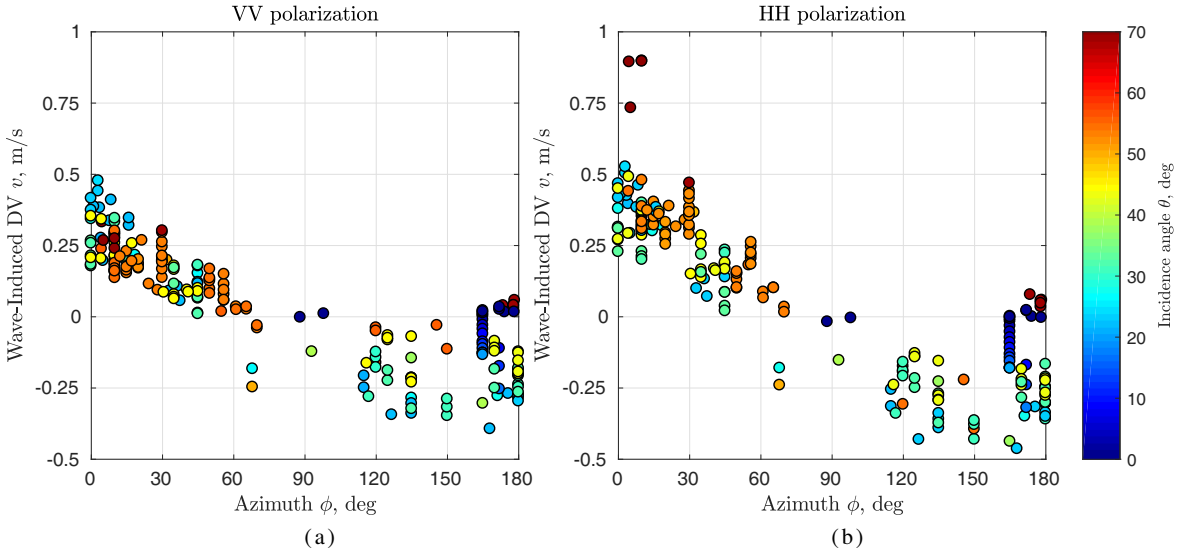

Figure 3: Measured Wave-Induced DV estimated from (4) versus radar-to-wave azimuth for (a) VV and (b) HH polarization.

wave phase velocity from $+c_{\rm br}$ to $-c_{\rm br}$ in this direction, which is subtracted from measured DV to estimate WIDV (4). Such sharp transition is the case for an isotropic Bragg wave azimuth spectrum but is not the case for a finite width angular spectrum.

At large incidence angles, $\theta = 70°$, and HH polarization, the simulated upwind WIDV is underestimated by a factor of ≈ 2 (Figs. 5(c), 5(d)). This indicates a contribution from breaking waves that are not accounted for in the WIDV estimate (4) and suggests the mean line-of-sight NRCS weighted breaker velocity of 0.3–0.5 m/s. At lower incidence angles, the wave breaking contribution decreases and the measured DV can be explained without wave breaking contribution.

4.3. Open ocean Simulation

Further, we attempt extrapolate the results obtained in fetch-limited conditions typical of the Black Sea to the open ocean conditions. Such estimates are obtained using the KMC spectrum in (7) without the low frequency truncation.

The sea surface spectrum has the universal frequency dependence, $S \sim f^{-5}$, and level in the

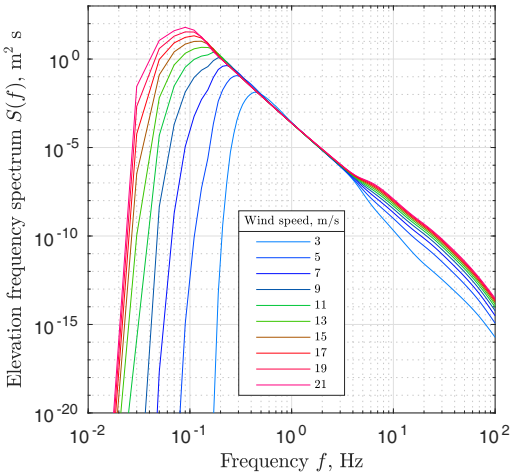

Figure 4: The omni-directional elevation spectrum, $S(f)$, simulated using KMC model [17].

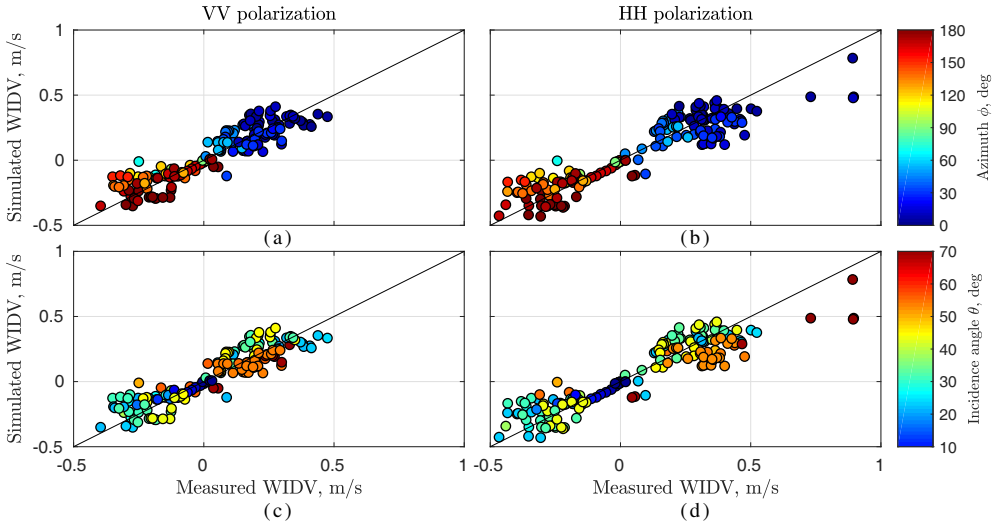

Figure 5: Scatter diagram of measured WIDV and WIDV simulated using KMC spectrum [17] for ((a), (c)) VV and ((b), (d)) HH polarization. Color scale corresponds to ((a), (b)) azimuth and ((c),(d)) incidence angle.

equilibrium range (Fig. 4) [24], thus the contribution of wave components to WIDV is inversely proportional to f^{-2}. The cumulative contribution of waves having frequencies lower than F,

$$q(F) = \frac{\int_0^F f^3 S(f) \mathrm{d}f}{\int_0^\infty f^3 S(f) \mathrm{d}f}, \tag{9}$$

in Fig. 6 reveals that more than 90% of the WIDV is produced by waves with $f < 2\,\mathrm{Hz}$ (wavelength $> 40\,\mathrm{cm}$). This means that WIDV is generally governed by the energy containing waves.

Simulated WIDV (Fig. 7) has a similar incidence angle, azimuth, and polarization dependences as those observed in the Black Sea (Fig. 2). With increasing wind speed, the WIDV grows in magnitude at small $\theta < 30°$, but decreases at larger $\theta > 30°$. Wind dependence of WIDV is controlled by the following two factors. MTF magnitude (7), and thus the WIDV, decreases with increasing wind speed [15]. But, the wave peak amplitude increases (faster orbital velocities) at higher winds, thus increasing the WIDV. The balance between the two factors controls the WIDV.

In the crosswind direction, the WIDV has a small negative magnitude of 0.2 m/s, which results from the specific MTF behavior observed in our Ka-band platform measurements [15, 20]. The NRCS peak appears to be shifted towards the rear (windward) slope of tilting wave. In the crosswind direction, the line-of-sight velocity is produced by the vertical component of orbital velocity and is

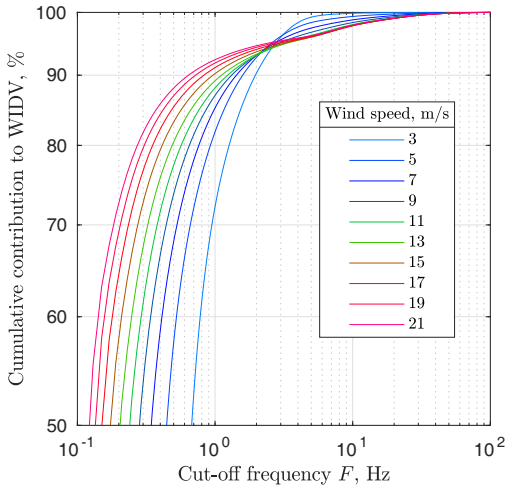

Figure 6: Cumulative contribution of wave frequency range ($0 < f < F$) to WIDV calculated using (9) for various winds.

equal in magnitude but opposite in sign on rear and forward slopes of tilting wave. But the rear slopes contribution dominates due to larger NRCS that leads to negative DV. For the same reason, the downwind WIDV is somewhat higher in magnitude than the upwind WIDV.

At given wind, the WIDV magnitude maximizes at $\theta \approx 20°$, where MTF magnitude also maximizes. Generally, HH WIDV is higher than VV WIDV. The difference between the two grows with wind speed and reaches 15–20 cm/s at $U = 15$ m/s.

As can be deducted from comparisons with Bragg wave phase velocity and expected wind drift (Fig. 7), the WIDV plays the crucial role at low incidence angles. At $\theta = 20°$ and $5 < U < 15$ m/s, it is 3–8 times larger than either Bragg or surface current contributions. At larger $\theta > 50°$, the relative role of WIDV component decreases, but it is still of the same order as Bragg and surface current components.

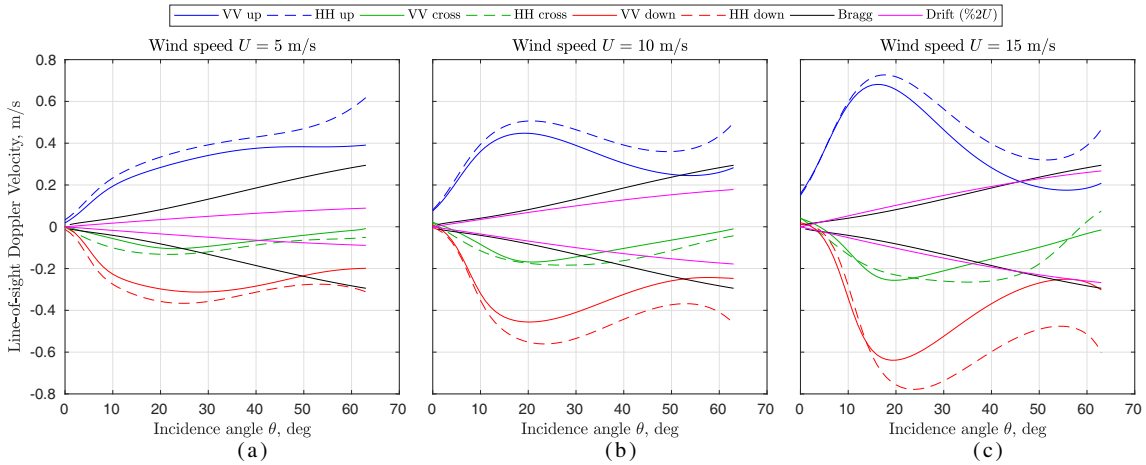

Figure 7: Wave-Induced DV versus incidence angle simulated for fully developed sea from KMC spectrum model [17] for wind speed (a) $U = 5$ m/s, (b) $U = 10$ m/s, and (c) $U = 15$ m/s.

5. SUMMARY

The paper presents an analysis of the sea surface Doppler velocity (DV) component arising due to the wave-induced correlation between local sea surface velocity and cross-section (referred to as the Wave-Induced Doppler Velocity, WIDV). The work is inspired by the growing interest in satellite Doppler measurements and prospects of retrieval of mesoscale ocean surface currents [2, 3].

From platform-based dual co-polarized Ka-band Doppler radar measurements of mean NRCS-weighted DV, we estimate the WIDV by subtracting the observed surface currents and the theo-

retical mean scatterer velocity (Bragg wave phase velocity). For fetch-limited wave state typical of the Black Sea, it is found that WIDV peaks at small incidence angles, $\theta \approx 20°$, with the magnitude of about 0.3–0.5 m/s. At high incidence angles, $\theta \approx 70°$, HH WIDV grows up to 0.8 m/s in the upwind direction.

Observed WIDV is compared to simulations that employ the empirical Ka-band radar Modulation Transfer Function (MTF) [15] and the Kudryavtsev *et al.* wind wave spectrum [17] truncated at $f < f_{\mathrm{p}}$ with the peak frequency, f_{p}, taken from wave gauge spectra. The agreement between the two WIDV is reasonable, except in the crosswind direction or at high incidence angles and HH polarization. In the crosswind direction, we attribute the deviation to the simplified azimuth dependence of Bragg phase velocity that sharply changes from $+c_{\mathrm{br}}$ to $-c_{\mathrm{br}}$. At large incidence angles and HH polarization, the wave breaking contribution should be accounted for.

Using the wind wave spectrum model [17] for fully developed sea, we extrapolate WIDV estimates into open ocean conditions. We found than about 90% of WIDV comes from the equilibrium range waves and longer (wave length > 40 cm). Resulting WIDV peaks at $\theta \approx 20°$ and its magnitude is 3 to 8 times larger than the contribution from either Bragg phase velocity or wind drift. The WIDV wind dependence is governed by the balance between the magnitude of wave orbital velocity, which grows with the wind, and the magnitude of MTF, which decreases with the wind.

The WIDV is apparently important to separate the surface current from the total DV. Its relative impact is stronger at small incidence angles, where wave-induced variations of NRCS are stronger. It seems that using larger incidence angles is preferable for more accurate surface current retrieval while the strong sensitivity of DV to wave parameters at small incidence angles can be used to improve the ocean wave retrievals.

ACKNOWLEDGMENT

The work was supported by the Russian Science Foundation grant 17-77-10052.

REFERENCES

1. Chapron, B., F. Collard, and F. Ardhuin, "Direct measurements of ocean surface velocity from space: Interpretation and validation," *Journal of Geophysical Research (Oceans)*, Vol. 110, No. C07008, doi:10.1029/2004JC002809, 2005.
2. Rodriguez, E., D. Perkovic-Martin, C. Baldi, K. Cooper, N. Majurec, M. Neumann, F. Nicaise, and G. Farquharson, "Ka-band doppler scatterometer for measurements of ocean surface vector winds and currents," *Proceedings of Earth Science Technology Forum ESTF2014*, Leesburg, Virginia, USA, October 2014.
3. Ardhuin, F., Y. Aksenov, A. Benetazzo, L. Bertino, P. Brandt, E. Caubet, B. Chapron, F. Collard, S. Cravatte, F. Dias, G. Dibarboure, L. Gaultier, J. Johannessen, A. Korosov, G. Manucharyan, D. Menemenlis, M. Menendez, G. Monnier, A. Mouche, F. Nouguier, G. Nurser, P. Rampal, A. Reniers, E. Rodriguez, J. Stopa, C. Tison, M. Tissier, C. Ubelmann, E. van Sebille, J. Vialard, and J. Xie, "Measuring currents, ice drift, and waves from space: The sea surface kinematics multiscale monitoring (SKIM) concept," *Ocean Science Discussions*, doi:10.5194/os-2017-65, 2017.
4. Thompson, D. R., *Calculation of Microwave Doppler Spectra from the Ocean Surface with a Time-Dependent Composite Model*, Springer, Dordrecht, Netherlands, 27–40, 1989.
5. Plant, W. J. "A model for microwave Doppler sea return at high incidence angles: Bragg scattering from bound, tilted waves," *Journal of Geophysical Research (Oceans)*, Vol. 102, 21131–21146, 1997.
6. Fois, F., P. Hoogeboom, F. Le Chevalier, and A. Stoffelen, "An analytical model for the description of the full-polarimetric sea surface doppler signature," *Journal of Geophysical Research: Oceans*, Vol. 120, No. 2, 988–1015, 2015.
7. Shibata, A., T. Uji, I. Isozaki, K. Nakamura, and J. Awaka, *Doppler Spectra of Microwave Radar Echo Returned from Calm and Rough Sea Surfaces*, Springer, Dordrecht, Netherlands, 263–268, 1985.
8. Hwang, P. A., M. A. Sletten, and J. V. Toporkov, "Analysis of radar sea return for breaking wave investigation," *Journal of Geophysical Research (Oceans)*, Vol. 113, No. C02003, doi: 10.1029/2007JC004319, 2008.
9. Mouche, A. A., F. Collard, B. Chapron, K. F. Dagestad, G. Guitton, J. A. Johannessen, V. Kerbaol, and M. W. Hansen, "On the use of doppler shift for sea surface wind retrieval from SAR," *IEEE Transactions on Geoscience and Remote Sensing*, Vol. 50, 2901–2909, 2012.

10. Hansen, M. W., V. Kudryavtsev, B. Chapron, J. A. Johannessen, F. Collard, K.-F. Dagestad, and A. A. Mouche, "Direct measurements of ocean surface velocity from space: Interpretation and validation," *Remote Sensing of Environment*, Vol. 120, 113–122, 2012.
11. Johannessen, J. A., B. Chapron, F. Collard, V. Kudryavtsev, A. Mouche, D. Akimov, and K.-F. Dagestad, "Direct ocean surface velocity measurements from space: Improved quantitative interpretation of Envisat ASAR observations," *Geophysical Research Letters*, Vol. 35, 22608, 2008.
12. Keller, W. C. and J. W. Wright, "Microwave scattering and the straining of wind-generated waves," *Radio Science*, Vol. 10, 139–147, 1975.
13. Feindt, F. , J. Schroter, and W. Alpers, "Measurement of the ocean wave-radar modulation transfer function at 35 GHz from a sea-based platform in the North Sea," *Journal of Geophysical Research (Oceans)*, Vol. 91, No. C8, 9701–9708, 1986.
14. Ermakov, S. A., I. A. Kapustin, V. N. Kudryavtsev, I. A. Sergievskaya, O. V. Shomina, B. Chapron, and Y. Y. Yurovskiy, "On the doppler frequency shifts of radar signals backscattered from the sea surface," *Radiophysics and Quantum Electronics*, Vol. 57, No. 4, 239–250, 2014.
15. Yurovsky, Y. Y., V. Kudryavtsev, S. A. Grodsky, and B. Chapron, "Normalized radar backscattering cross-section and doppler shifts of the sea surface in ka-band," *Proceedings of "Progress in Electromagnetic Research Symposium"*, Saint-Petersburg, Russia, May 2017.
16. Longuet-Higgins, M. S. "The statistical analysis of a random, moving surface," *Royal Society of London Philosophical Transactions Series A*, Vol. 249, 321–387, 1957.
17. Kudryavtsev, V. N., V. K. Makin, and B. Chapron, "Coupled sea surface-atmosphere model: 2. spectrum of short wind waves," *Journal of Geophysical Research: Oceans*, Vol. 104, No. C4, 7625–7639, 1999.
18. Kudryavtsev, V., D. Hauser, G. Caudal, and B. Chapron, "A semiempirical model of the normalized radar cross-section of the sea surface 1. Background model," *Journal of Geophysical Research (Oceans)*, Vol. 108, No. C08054, doi: 10.1029/2001JC001003, 2003.
19. Yurovskaya, M. V., V. A. Dulov, B. Chapron, and V. N. Kudryavtsev, "Directional short wind wave spectra derived from the sea surface photography," *Journal of Geophysical Research (Oceans)*, Vol. 118, 4380–4394, 2013.
20. Yurovsky, Y. Y., V. N. Kudryavtsev, S. A. Grodsky, and B. Chapron, "Ka-band dual copolarized empirical model for the sea surface radar cross section," *IEEE Transactions on Geoscience and Remote Sensing*, Vol. 55, No. 3, 1629–1647, 2017.
21. Doviak, R. J. and D. S. Zrnic, *Meteorological Radar Signal Processing*, 91–120, Academic, San Diego, USA, 1984.
22. Donelan, M. A., J. Hamilton, and W. H. Hui, "Directional spectra of wind-generated ocean waves," *Philosophical Transactions of the Royal Society of London A: Mathematical, Physical and Engineering Sciences*, Vol. 315, No. 1534, 509–562, 1985.
23. Cox, C. and W. Munk, "Measurement of the roughness of the sea surface from photographs of the sun's glitter," *Journal of the Optical Society of America*, Vol. 44, 838–850, 1954.
24. Phillips, O. M., *Dynamics of the Upper Ocean*, Cambridge University Press, 1977.